Conversion of NO to N_2O on MgO Thin Films

Cristiana Di Valentin and Gianfranco Pacchioni*

Dipartimento di Scienza dei Materiali, Istituto Nazionale per la Fisica della Materia, Università di Milano-Bicocca, via R. Cozzi 53, I-20125 Milano, Italy

Stéphane Abbet and Ueli Heiz

Institute of Surface Chemistry and Catalysis, University of Ulm, D-89069 Ulm, Germany

Received: March 15, 2002; In Final Form: May 14, 2002

Adsorption of NO on MgO ultrathin films grown on a Mo(100) substrate results in the formation of N_2O at low temperature (120 K). In addition, small amounts of N_2O are produced at 280 K. Isotope exchange experiments show that the reaction does not involve lattice oxygens. Ab initio DFT/B3LYP cluster model calculations have been performed to understand the mechanism of the reaction. Various defect sites on the MgO surface have been considered. It is found that the reaction occurs preferentially at neutral oxygen vacancies (F centers) through the adsorption of a first NO molecule followed by the addition of a second NO; from the adsorbed dimer, N_2O_2, N_2O forms with an activation barrier of about 0.1 eV, leaving a regular site instead of the original F center. This result is consistent with the experimental observation that subsequent exposure of the surface to NO results in a reduced production of N_2O.

1. Introduction

Adsorption processes associated with nitric oxide, NO, at metal oxide surfaces are a subject of great importance and continuous research in the context of heterogeneous catalysis. NO, spontaneously produced in combustion processes at high temperature, is highly toxic and has to be removed from the car exhaust gases through reduction to N_2. It has been observed that, besides many well-characterized metal catalysts,[1−5] alkaline-earth-metal oxide surfaces are also able to increase the rate of this reaction.[6−10]

During NO exposure of prereduced CaO powders at low temperatures (between room temperature and 500 °C) both N_2 and N_2O are formed.[8,10] At high temperatures (above 500 °C) CaO further catalyzes N_2O decomposition to N_2.[11,12] Low-temperature formation of N_2O has also been detected, through infrared spectroscopy on MgO powders at 77 K[6] and through thermal desorption spectroscopy on MgO thin films grown on Mo(100) at 90 K.[13,14] The temperature-programmed desorption (TPD) spectrum is characterized by an intense peak at 120 K and a weak one at 280 K, indicating two possible reaction mechanisms, characterized by different activation barriers.

In principle, as is observed in the case of metal surfaces, NO could chemisorb in both molecular and dissociative forms. Although there is no definitive proof that NO dissociation can be ruled out as a viable and competitive reaction channel, only NO molecular chemisorption is generally proposed for alkaline-earth-metal oxides.[6,8−10,15,16] This first reaction step is followed by formation of NO dimers (second reaction step) and disproportionation to N_2O and O adsorbed onto the surface (third reaction step). In the case of CaO, surface F_s centers, oxygen vacancies with trapped electrons, have been considered as possible oxygen traps, which are able to decompose NO dimers and to induce the formation of N_2O. Such a route is noncatalytic and is possible only with the assumption of a prereduced surface.[8,10] Some computational data on the thermodynamics of the process, however, are in favor of this hypothesis.[15] For MgO surfaces, experimentalists[6] and theoreticians[16] have proposed a reaction channel in which NO dimers react with low-coordinated anionic sites, producing N_2O and surface peroxide species. However, we believe that the route involving oxygen vacancies is definitely plausible also for the MgO system, which despite being less reactive presents many similarities to CaO.

NO dimer formation is the second step of the reaction for all possible chemisorption sites. Gas-phase dimerization is characterized by a very small energy gain, 0.14 eV, and by a long N−N bond, 2.363 Å.[17−19] The same is true also for dimerization on MgO cationic sites.[13,16] These features are not reassuring in view of forming a triple N−N bond in the N_2O molecule. It was shown however that anionic dimeric species such as $(N_2O_2)^-$ and $(N_2O_2)^{2-}$ present a much shorter N−N bond, typical of the N−N double bond.[20] Therefore, the presence of excess electrons on the adsorption site is essential to activate adsorbed precursors for the production of molecular N_2O. F_s centers are not the only possible surface sites with electrons available for chemical reactions. We have already mentioned the low-coordinated anionic sites, and one can also think of other shallow electron traps such as, for example, some morphological sites.[21]

In the present experimental and quantum mechanical study we aim, on one side, at analyzing the conversion of NO to N_2O on well-characterized thin films of MgO(100) through thermal desorption spectroscopy (TDS) and Fourier transform infrared (FTIR) spectroscopy and, on the other side, at defining the geometries and relative energies for intermediates and transition structures (TSs) through density functional theory (DFT) calculations. On the basis of the thermodynamic data it is possible to discuss the potential role of the direct dissociative process and evaluate the energy of adsorption and dimerization. Moreover, the comparison of the activation barriers for the

* To whom correspondence should be addressed. E-mail: gianfranco.pacchioni@unimib.it.

10.1021/jp0207127 CCC: $22.00
Published on Web 07/13/2002

disproportionation to N_2O and O is used to discuss the reactivity of the different sites toward NO reduction. In particular we are interested in

(i) assessing the various reaction steps on the F_s centers,

(ii) determining the effect of coordination on the F_s reactivity,

(iii) evaluating the different behavior of F_s and F_s^+ centers, in the presence of one or two trapped electrons, respectively,

(iv) evaluating the ability of other electron traps to catalyze the reaction, and

(v) establishing the activation barrier for the process on the low-coordinated anions.

The paper is organized as follows. In section 2 we present the experimental and computational details. In section 3 we discuss the experimental results. Section 4 is dedicated to the description of the calculations. Conclusions are given in the last section.

2. Experimental and Computational Details

2.1. Experimental Details. The conversion of NO to N_2O was studied experimentally on well-characterized thin films of MgO(100). They are grown on Mo(100) single crystals by evaporating pure metallic magnesium in an oxygen background of 5×10^{-7} mbar. Subsequently they are annealed to 840 K. Auger electron spectroscopy (AES) measurements show a one-to-one stoichiometry of the films and the absence of any impurities.[22] Typical thicknesses were about 10 monolayers (MLs), as determined by AES peak intensities and by X-ray photoemission (XPS) using the intensity attenuation of the Mo 3d core level with increasing film coverage.[23]

Low-energy electron diffraction (LEED) taken of a MgO film after a short annealing shows a sharp (1×1) pattern.[23] Multiple phonon losses in the high-resolution energy loss spectrum (HREELS), the characteristic ultraviolet photoelectron spectrum (UPS) from the O 2p valence band, and electron energy loss spectra (EELS) with the characteristic loss at about 6 eV[23] indicate a well-ordered MgO(100) single-crystal surface in good agreement with previous studies.[24−28]

Although these MgO(100) films reveal properties similar to those observed for the corresponding three-dimensional solids, they expose, depending on the Mg evaporation rate, O_2 background pressure, and annealing temperature, a reproducible density of defects on their surface. These defects are characterized by the adsorption properties of small molecules. For CO chemisorption on MgO(100) it was concluded from highly accurate first-principle theoretical model calculations[29] that the relatively strong chemisorption energy coupled with an unusual blue shift of the CO frequency in CO/MgO(100)/Mo(100) reported experimentally[30] cannot correspond to chemisorption on regular, unperturbed five-coordinated sites as claimed.[31,32] Rather, it was suggested that the unusually strong interaction should be connected with extended defects (steps, kinks) on the oxide film. In addition to the extended defect sites, oxygen vacancies (F centers) could be detected.[33] The existence of F centers is deduced from the good agreement of experimental and theoretical binding energies and vibrational frequencies of CO adsorbed to single Pd atoms trapped on the point defects. Scanning tunneling microscopy (STM) measurements of a 2 ML MgO/Ag(001) thin film, epitaxially grown at 500 K, also point to the existence of F centers.[34]

The in situ prepared films were then exposed to 5 langmuirs of ^{15}NO with a calibrated molecular beam doser. The adsorption of NO and the formation of N_2O were characterized by using TDS and FTIR spectroscopy. For the TDS experiments, a heating rate of 2 K/s was used and the desorbing molecule was detected with a differentially pumped mass spectrometer (Balzers QMS 420) after electron impact (70 eV) ionization. The infrared spectra were measured in single-reflection mode where the infrared beam is focused at a grazing angle (85°) onto the sample. The reflected beam was detected by a narrow-band mercury cadmium telluride (MCT) detector. A total of 512 interferograms were averaged, and no smoothing of the spectra was performed.

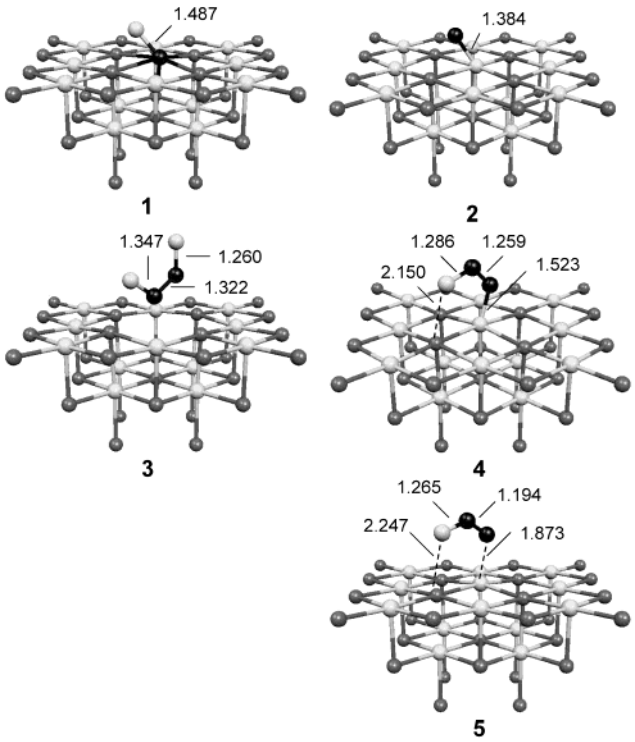

Figure 1. $[Mg_5O_{12}ECP_{14}]$ cluster model of a neutral oxygen vacancy, F center, at a terrace site interacting with one NO molecule (**1** and **2**) and two NO molecules (**3** and **4**). In **5** is shown the transition state for the reaction $N_2O_2 \rightarrow O_{ads} + N_2O$. Key: gray spheres, Mg; white spheres, O; black spheres, N. Selected distances are given in angstroms.

2.2. Theoretical Aspects. The interaction of NO monomers and dimers with neutral and positively charged oxygen vacancy sites, neutral surface electron traps, and low-coordinated anionic sites has been studied by means of cluster models.[35] This approach has been widely used to study the adsorption and the reaction of gas-phase molecules with oxide surfaces.[36,37] The truncation of the lattice in cluster models of ionic materials implies the use of external fields to represent the long-range Coulomb potential.[38] In this work we use large arrays of point charges (PCs) to reproduce the Madelung potential at the adsorption site. Previous studies have demonstrated that a disadvantage of this technique is the artificial polarization of the oxygen anions of the cluster, resulting from the presence of the nearest-neighbor positive PCs and causing an incorrect behavior of the electrostatic potential in the adsorption region.[39] This problem can be circumvented by placing effective core potentials (ECPs), in particular the CEP[40,41] ECPs, instead of positive PCs at the cluster borders.[42−44] The cluster approach is computationally simple and parameter free and has been shown to properly describe the physics of local surface processes.[35,45]

The neutral F_s and charged F_s^+ oxygen vacancies have been modeled by a $[Mg_5O_{12}ECP_{14}]$ cluster surrounded by 645 PCs (terrace site, Figure 1 and Figure 3) and by a $[Mg_{10}O_{11}ECP_{16}]$ cluster surrounded by 600 PCs (edge site, Figure 2). For the

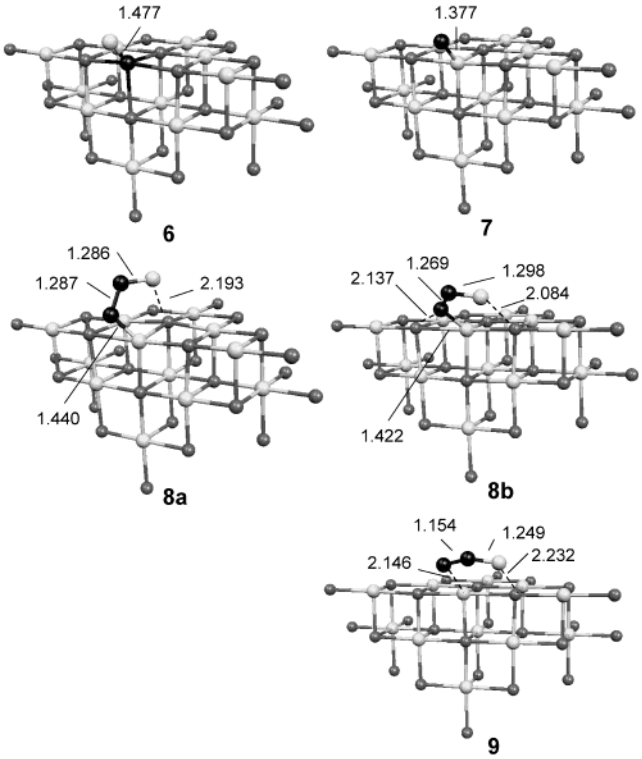

Figure 2. $[Mg_{10}O_{11}ECP_{16}]$ cluster model of a neutral oxygen vacancy, F center, at an edge site, interacting with one NO molecule (**6** and **7**) and two NO molecules (**8a** and **8b**). In **9** is shown the transition state for the reaction $N_2O_2 \rightarrow O_{ads} + N_2O$. Key: gray spheres, Mg; white spheres, O; black spheres, N. Selected distances are given in angstroms.

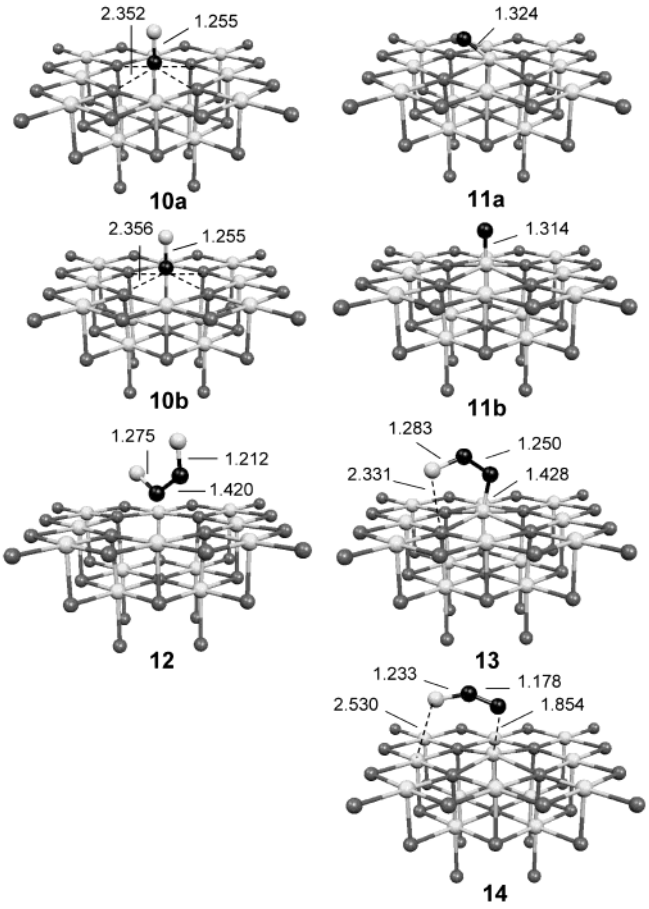

Figure 3. $[Mg_5O_{12}ECP_{14}]$ cluster model of a charged oxygen vacancy, F^+ center, at a terrace site interacting with one NO molecule (**10** and **11**; **a**, singlet state; **b**, triplet state) and two NO molecules (**12** and **13**). In **14** is shown the transition state for the reaction $N_2O_2 \rightarrow O_{ads} + N_2O$. Key: gray spheres, Mg; white spheres, O; black spheres, N. Selected distances are given in angstroms.

reverse corner we used a $[O_{10}Mg_{15}ECP_9]$ cluster surrounded by 652 PCs (Figure 4). The low-coordinated O^{2-} edge site is represented by a $[Mg_{10}O_{10}ECP_{14}]$ cluster surrounded by 604 PCs (Figure 5). Ions, ECPs, and PCs taken together are electrically neutral.

The calculations were performed at the DFT level. Becke's three-parameter hybrid exchange functional[46] in combination with the gradient-corrected correlation functional of Lee, Yang, and Parr,[47] generally referred to as B3LYP, has been used. Geometry optimization was computed by means of analytical gradients with no symmetry constraints. The eight O anions and the four Mg cations of the first layer of the cluster have been relaxed for the terrace and edge F_s centers. In the case of the reverse corner we optimized the position of all those anions and cations, which are not in direct contact with the PCs. For the edge adsorption site only the interacting oxygen and the closest Mg ion positions were relaxed. Spin-polarized calculations have been performed to take into account open-shell configurations.

The basis set for the five Mg^{2+} ions adjacent to the vacancy is 6-31+G*, including diffuse functions, with no additional basis functions located at the vacancy center.[48] All the remaining Mg cations and O anions have been treated with a 6-31G basis set. The NO monomer and dimer were described with a 6-31+G* basis set. In a previous work we showed that there is no need for ghost functions at the vacancy center to describe the localization of trapped electrons, since a good description can be achieved with the use of standard basis functions of reasonable quality (such as at least 6-31+G).[48]

The calculations have been performed using the Gaussian-98 program package.[49]

3. Results and Discussion

3.1. Experimental Results. MgO ultrathin films grown on a Mo(100) substrate have been exposed to ^{15}NO at 95 K in an ultrahigh-vacuum (UHV) chamber. A narrow desorption peak for $m/z = 31$ amu is detected with a maximum desorption rate at 100 K (not shown in this work). In addition, a small desorption signal is observed at 450 K. The desorption at 100 K is attributed to residual desorption of ^{15}NO dimers from terrace sites and NO monomers from extended defect sites. The desorption at 450 K results from chemisorbed ^{15}NO species on point defects.[50] These results are in qualitative agreement with those obtained by the group of Goodman.[14]

At the same ^{15}NO exposures FTIR spectra were recorded at 95 K. Three bands at 1862, 1778, and 1747 cm^{-1} are observed in Figure 6a. After the sample is annealed to 150 K they completely disappear. If we take into account the isotope effect, 34 cm^{-1}, and refer our values to ^{14}NO, the bands are at 1896, 1812, and 1781 cm^{-1}, respectively. We note that the absorption bands in Figure 6a are very small with respect to the amount of absorbed NO. This indicates that the axis of the NO molecule is tilted with respect to the surface normal. In both cases one component of the spectrum is blue-shifted with respect to the band of free NO (free molecule experimental frequency, $\omega_e = 1876$ cm^{-1}; the harmonic frequency, ω_0, is estimated to be 1904 cm^{-1}).[18] The frequencies of these bands are close to those obtained by Zecchina et al.[6] for the adsorption of NO onto MgO

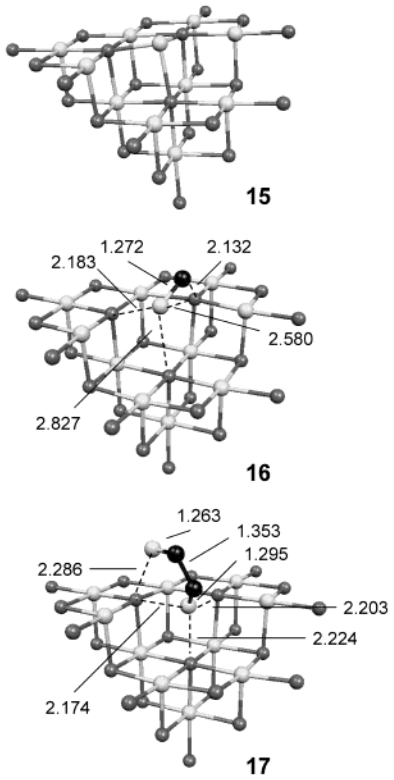

Figure 4. $[O_{10}Mg_{15}ECP_9]$ cluster model of a shallow electron trap at the MgO surface, consisting of one electron localized at a reverse corner site, interacting with one O atom (**15**), one NO molecule (**16**), and two NO molecules (**17**). Key: gray spheres, Mg; white spheres, O; black spheres, N. Selected distances are given in angstroms.

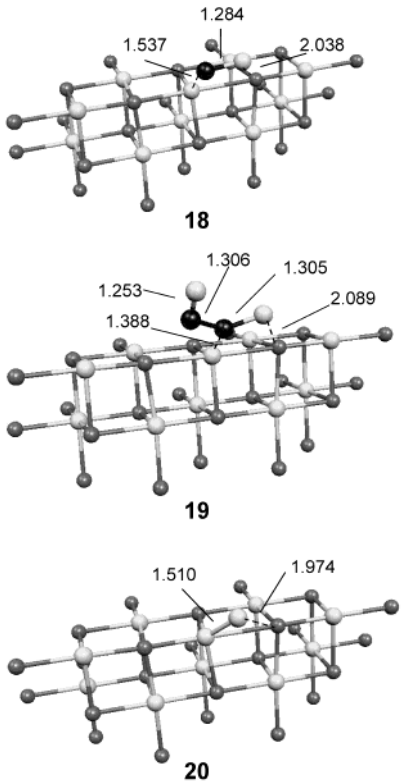

Figure 5. $[Mg_{10}O_{10}ECP_{14}]$ cluster model of a low-coordinated O anion at an edge site, interacting with one NO molecule (**18**), two NO molecules (**19**), and a single adsorbed O atom (**20**). This latter structure corresponds to the formation of a surface peroxo species. Key: gray spheres, Mg; white spheres, O; black spheres, N. Selected distances are given in angstroms.

microcrystals. According to Zecchina et al.[6] the spectrum obtained for NO on MgO powders is the superposition of two pairs of bands assigned to *cis*-N_2O_2 species, adsorbed onto two different surface sites. Each pair of bands is due to the symmetric and the antisymmetric stretching modes of N_2O_2. Therefore, we assign the blue-shifted band (1862 cm^{-1}) to the symmetric stretch mode of N_2O_2.[13]

Besides the molecular desorption of ^{15}NO and most important for this work, the TDS experiment reveals the formation of $^{15}N_2O$. This points toward the presence of reactive sites on the MgO thin films. $^{15}N_2O$ desorbs at 120 K, and a small amount of this species also desorbs at around 280 K (Figure 6b). Under none of the experimental conditions, however, vibrational features typical for adsorbed $^{15}N_2O$ could be observed (Figure 6a). This suggests that the formed N_2O directly desorbs from the surface after formation and the desorption temperature can be attributed to the temperature of formation. In this context, it is interesting to investigate whether surface oxygen is involved in any reaction path. For this $Mg^{18}O$ films were produced by evaporating Mg in an $^{18}O_2$ background (5×10^{-7} mbar). If the MgO surface is involved, ^{18}O-containing species should be detected. No such species could be observed in our TDS experiments. To elucidate further the character of the active site for the formation of $^{15}N_2O$ on the MgO thin film, we performed several adsorption−desorption cycles for ^{15}NO. Figure 6b shows the first TPD spectrum after film preparation for $m/z = 46$ amu ($^{15}N_2O$). After ramping up to 450 K the same amount of ^{15}NO was adsorbed at 95 K, and the resulting TPD spectrum is shown in Figure 6c. A comparison of the peak heights clearly shows that formation of $^{15}N_2O$ has diminished. This result indicates that the reactive site is poisoned upon reaction. A possible explanation is that the reactive sites are F centers, which are annealed after disproportionation of N_2O_2 to N_2O and O. This is also consistent with the absence of molecular oxygen desorbing from the surface during the reaction. The decrease of the N_2O production with time, the absence of molecular oxygen formation, and the temperature of N_2O desorption of 120 K allow one to exclude the alternative reaction mechanism of N_2O_2 species, weakly bound on terrace sites, to form N_2O and atomic O, given that these dimers desorb already at 100 K into NO monomers.[13]

3.2. Computational Results. *3.2.1. Gas-Phase N_2O_2, $(N_2O_2)^-$, and $(N_2O_2)^{2-}$.* Before analyzing the reactivity of NO dimers on the defective MgO surface, we report some data on the various gas-phase species. The neutral NO dimer, N_2O_2, is more stable in the triplet state, and is characterized by a very weak binding energy, 0.14 eV,[18] and a long N−N bond, 2.263 Å.[17] Unrestricted B3LYP/6-31+G* calculations result in a weakly unbound state by 0.02 eV, with a N−N bond length of 1.96 Å, and an almost unperturbed NO bond of 1.16 Å, in line with previous studies. The formation of a distance of less than 2 Å despite the fact that the system is unbound is indicative of the existence of a local minimum on the potential energy surface.

The addition of one electron to the dimer, $(N_2O_2)^-$, reinforces the N−N bond (1.41 Å) and slightly weakens the N−O bond (1.26 Å). The effect of a second electron is to fill the N−N π bonding level, resulting in a short N−N bond (1.30 Å) and a longer N−O bond with a single-bond character (1.35 Å). Therefore, the presence of an excess of electronic charge on the molecule on one side activates the N−O bond breaking, which is required to produce the N_2O molecule, and on the other strengthens the N−N bond, which has to be formed. For this reason electron-rich sites on the MgO surface should be ideal to promote NO reduction to N_2O. In fact, in a recent paper we

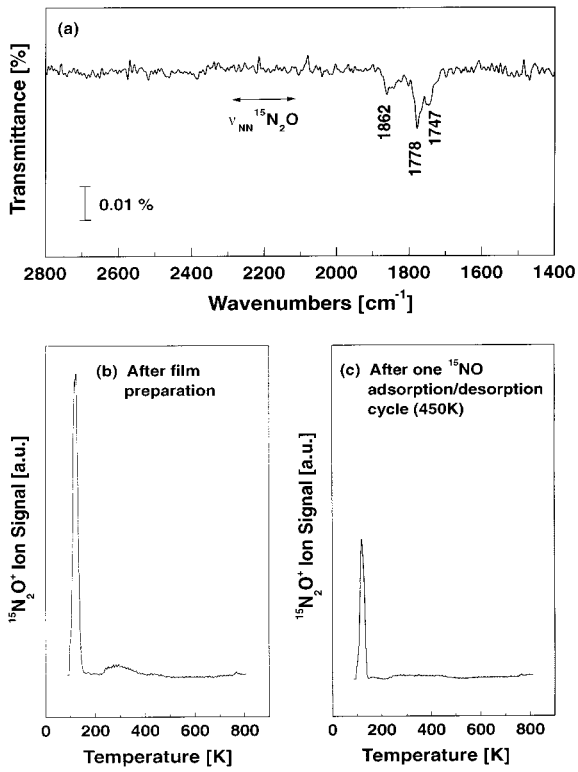

Figure 6. (a) Infrared spectrum of NO adsorbed onto a MgO thin film grown on Mo(100). The spectrum was taken at 90 K. Note that there is no infrared absorption in the region of $\nu_{NN}(N_2O)$. (b) TDS spectrum showing $^{15}N_2O$ formation after exposure of a freshly prepared MgO film to 5 langmuirs of NO. (c) TDS spectrum of $^{15}N_2O$ formation after a ^{15}NO adsorption−desorption cycle. In this cycle the film was annealed up to 450 K.

have shown that N_2O_2 species adsorbed onto nondefective terrace sites present a long N−N bond (1.81 Å) and a short NO bond (1.17 Å),[13] which are unfavorable conditions for N_2O formation.

It must be mentioned that while the electron affinity, EA, of the N_2O_2 molecule is high and positive[20] (EA = 2.0 eV calculated with B3LYP/6-31+G*), there is a significant energy cost to add a second electron (EA = −2.2 eV). Therefore, $(N_2O_2)^{2-}$ is not a stable species and its localization as a minimum on the potential surface can be explained only by the use of a finite basis set. However, when adsorbed onto the MgO surface, the anionic species can be stabilized by the local potential.

3.2.2. Terrace F_s Centers. We first looked at the interaction of NO monomers with the neutral oxygen vacancy on the MgO terrace, F_s. This site is characterized by the presence of two electrons trapped in the vacancy. The NO molecule does not physisorb on the top of the F_s center but, after geometry relaxation, fills the oxygen vacancy either with the nitrogen (see **1** in Figure 1) or the oxygen (**2**) atom and the other atom lying above the surface, tilting on one side to improve the electrostatic interaction with the Mg cations (Figure 1). Notice that structure **2** corresponds to that obtained by adsorbing a neutral N atom onto a surface O anion. The resulting NO bond length (**1**, 1.384 Å; **2**, 1.487 Å) is elongated with respect to that of gas-phase NO (1.16 Å). The binding energies for the two possible approaches, N-down or O-down, are identical, 3.8 eV, and are quite high since one of the two atoms is completely inserted into the crystal lattice, thus contributing to the high stabilization due to the Madelung potential.

SCHEME 1

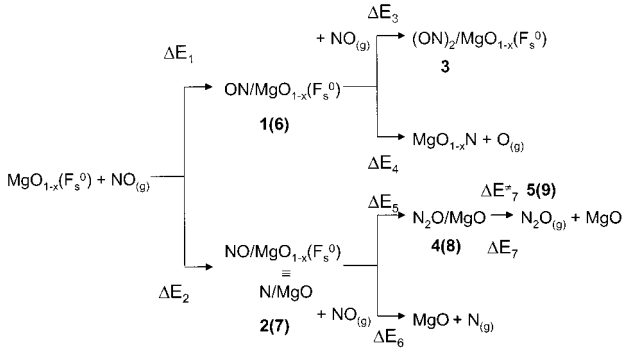

The addition of the second NO molecule to complexes **1** and **2** is an exothermic reaction leading to **3** and **4** (Figure 1). The energetics are different in the two cases (see also Scheme 1), $\Delta E_3 = -1.82$ eV and $\Delta E_5 = -3.73$ eV, respectively, reflecting the structural differences. Both N_2O_2 species absorbed on the defective surface are in the *cis* conformation. However, while for the O-down orientation (**2**) the addition of the second NO molecule does not alter the oxygen position, still inserted into the surface plane (**4**), for the N-down orientation (**1**) the addition of the second NO molecule modifies the position of the nitrogen atom which lies above the surface plane (see **3** in Figure 1). This geometry variation is due to the fact that the adsorption of the second NO molecule implies the formation of a N−N bonding which is hindered when the N atom of the first NO molecule is completely inserted into the vacancy.

The two electrons of the vacancy are transferred to the dimer, leading to a singlet state. This becomes clear by analyzing the geometrical parameters of the adsorbed molecule. The effect of the first added electron is to drastically reduce the N−N bond length, with respect to that of gas-phase N_2O_2, from almost 2 to 1.26−1.32 Å, depending on the orientation. The effect of the second electron transferred is to elongate the NO bond from 1.16 Å in the gas phase to 1.26 and 1.35 Å for **3** and to 1.29 and 1.52 Å for **4**. The activation of the NO_{ads} bond is essential when the reaction to produce N_2O is considered.

This finding has triggered the search for the TS leading to the perfect surface plus a N_2O molecule. The localization of this TS is not straightforward since not all degrees of freedom can be optimized in the TS search. The critical point can be considered a first-order saddle point only with respect to the variables that can be relaxed. The eigenvector corresponding to the characterizing negative eigenvalue of such a TS correctly involves the stretching mode of the breaking NO bond. Consequently, the localized TS **5** (Figure 1) presents a NO bond (1.873 Å) longer than that measured in the minimum (1.523 Å for **4**).

Let us now discuss the energetics. In Scheme 1 we summarized the possible reaction routes and the various reaction steps. The reaction energies are reported in Table 1. As we mentioned above, the NO monomer adsorption onto the vacancy is independent of the NO orientation ($\Delta E_1 = \Delta E_2 = -3.8$ eV). Once the NO has adsorbed in the N-down orientation, we consider two possible routes: (a) NO dissociation and (b) NO dimerization. The former is endothermic, $\Delta E_4 = 5.03$ eV, while the latter is exothermic, $\Delta E_3 = -1.82$ eV. The products of dissociation (a) are the filled surface and the gas-phase released atom (oxygen in this case). The oxygen atom can subsequently chemisorb on a surface oxygen anion, forming a peroxo species $(O_2)^{2-}$ with an adsorption energy of 2.18 eV. Thus, the total energy required to detach an O atom from adsorbed NO and

TABLE 1: Reaction Energies and Activation Barriers (eV) for the Various Steps Illustrated in Schemes 1 and 2

	ΔE_1	ΔE_2	ΔE_3	ΔE_4	ΔE_5	ΔE_6	ΔE_7	$\Delta E^{\ddagger}_7$
terrace F_s^0	−3.84	−3.83	−1.82	5.03	−3.73	1.16	−0.14	0.10
edge F_s^0	−3.08	−2.45	−4.48	4.78	−5.11	0.58	0.05	0.72
terrace F_s^+	−2.79	−2.82	−0.49	5.81	−1.28	3.57	−0.18	0.41

adsorb it onto an O^{2-} anion on a terrace is positive by ∼3 eV. Also when the NO molecule adsorbs in the O-down orientation, we can expect (a) dissociation and (b) dimerization. Again the former is an endothermic reaction ($\Delta E_6 = 1.16$ eV), while the latter is exothermic ($\Delta E_5 = -3.73$ eV). After dissociation the released N atom could adsorb onto another surface oxygen anion, with a stabilization energy of 1.16 eV, resulting in a thermoneutral process (but presumably with a high activation barrier). After dimerization has taken place, N_2O production is possible through activation to TS **5**, overcoming a very small barrier ($\Delta E^{\ddagger}_7$) of only 0.10 eV. The product formation is also characterized by a small energy gain, $\Delta E_7 = -0.14$ eV, which should be compared to that of the gas-phase dissociation of N_2O_2 to $N_2O + O_{ads}$, endothermic by 1.49 eV.

To summarize, NO monomer adsoption on a terrace F_s center on the terrace can follow two possible orientations. In both orientations dimerization is preferred with respect to NO dissociation, but the dimer with the oxygen inserted into the vacancy presents a higher stabilization energy. From this intermediate, disproportionation to form N_2O is easily achieved even at low temperature given the very small barrier involved in the reaction. This is consistent with the experimental observation of N_2O formation at a low temperature and with the fact that subsequent exposure of the surface to NO results in a reduced activity because of the progressive quenching of the active centers.

3.2.3. Edge F_s Centers. In this section we analyze a low-coordinated F_s center, in the edge position on the surface (Figure 2), to evaluate the effect of the low coordination on the reactivity toward NO monomers and dimers. As for the terrace F_s center, the NO molecule does not physisorb on the top of the vacancy but one of the two atoms of the molecule is completely inserted into the vacancy. It is surprising that the N-down orientation, **6**, is even more stable than the O-down orientation, **7**, by 0.6 eV. The NO bond elongation is very similar to that of the terrace F_s center (**6**, 1.377 Å; **7**, 1.477 Å; Figure 2). The addition of the second NO molecule leads to two possible dimers (**8a** and **8b**), with similar adsorption energies (4.50 and 5.11 eV, respectively). Note that when we start the geometry optimization from one NO molecule added to the N-down complex, **6**, we observe a rearrangement of the molecule, resulting in an O-down orientation. The geometry parameters of the two minima, **8a** and **8b**, are very similar and characteristic of a $(N_2O_2)^{2-}$ species: a very short N−N distance with double-bond character (**8a**, 1.287 Å; **8b**, 1.269 Å) and a quite activated NO_{ads} bond (1.422 and 1.440 Å, respectively), but less than in the case of adsorption onto the neutral terrace F_s center. We limited the TS search to the most stable dimer complex, **8b**. We localized a TS with the proper eigenvector describing the NO stretching mode motion. The breaking NO bond is 2.146 Å (TS **9**). The geometrical features of the N_2O fragment are very close to those of the free N_2O molecule.

Referring again to Scheme 1 and Table 1, we can summarize the energetics of the catalyzed N_2O production on edge F_s centers. The monomer adsorption onto the oxygen vacancy in the N-down orientation is favored by ∼0.6 eV ($\Delta E_1 - \Delta E_2$). The addition of the second NO molecule (dimerization) is favored with respect to dissociation: the elimination of the O atom is endothermic by 4.78 eV (ΔE_4), and the elimination of the N atom is endothermic by 0.58 eV (ΔE_6), while the dimerization to **8a** and **8b** is exothermic by at least −4.5 eV (ΔE_5).

The activation barrier ($\Delta E^{\ddagger}_7$) for the formation of N_2O from the dimer is only 0.72 eV, and the products are slightly higher in energy than the adsorbed dimer ($\Delta E_7 = 0.05$ eV, to be compared to the value for the gas-phase reaction, $N_2O_2 \rightarrow N_2O + O$, 1.49 eV).

Also in the case of the neutral edge F_s center, there are two possible orientations for NO adsorption. Dimerization is preferred to dissociation, but is observed only in the O-down orientation. The activation barrier for the production of N_2O is higher than that obtained for the neutral F_s center at a terrace. Therefore, we can conclude that the effect of low coordination on F_s is to reduce the reactivity. This is consistent with the fact that low-coordinated F_s centers bind adsorbed species more strongly, hence resulting in higher energy barriers. This result also indicates that F_s centers at the MgO(100) terraces are more likely to be involved in the reaction than the corresponding low-coordinated defects. This conclusion is fully consistent with the analysis of the energetics of the reaction of acetylene cyclization occurring on Pd atoms stabilized at MgO defect centers.[51]

3.2.4. Terrace F_s^+ Centers. The analysis of the F_s^+ center is important to clarify the effect of reducing the number of electrons available in the oxygen vacancy. The presence of only one electron in the vacancy results in two possible spin multiplicities for the F_s^+/NO complexes: singlet and triplet. We localized the minima through optimization of the geometry for both spin states. Notice that the triplet states (**b**) are more stable than the singlet ones (**a**) (see below). In the singlet state the N-down and O-down orientations are quite different, Figure 3. The N atom of the singlet species **10a**, N-down, is not inserted into the vacancy site, but lies slightly above the surface plane with a distance from the Mg cations of 2.352 Å. The NO bond length is quite short with respect to that obtained for the other sites and only slightly longer than in free NO; moreover, the NO molecule is normal to the surface and not tilted as for adsorption onto the F_s center. This is likely to be due to the alignment of the NO dipole with the component of the electric field normal to the surface. The triplet state **10b** looks exactly the same as the singlet. Species **11a**, O-down, in the singlet state is very similar to that obtained for the F_s center, except that the tilting is larger, the NO bond elongation is less pronounced, and the O atom sits slightly above the surface plane. The triplet state with O-down orientation, **11b**, differs from the singlet in the absence of tilting.

The addition of a second NO molecule, resulting in a doublet state, leads to two structures, **12** and **13**, which are similar to those obtained for the neutral F_s center. A closer look at the geometrical parameters is important to understand the energetics of the reaction steps. The excess electron is transferred to the N_2O_2 fragment according to the Mulliken spin distribution, and the N−N bond is shortened to a value close to that of a double bond (∼1.3 Å). However, this is not sufficient to reach the same NO bond activation obtained with two excess electrons (F_s centers). In **13** the NO_{ads} bond length is 1.428 Å vs 1.523 Å in **4**; in **12** it is 1.275 Å vs 1.347 Å in **3**. The structural parameters of the TS toward N_2O formation, **14**, are very close to those

SCHEME 2

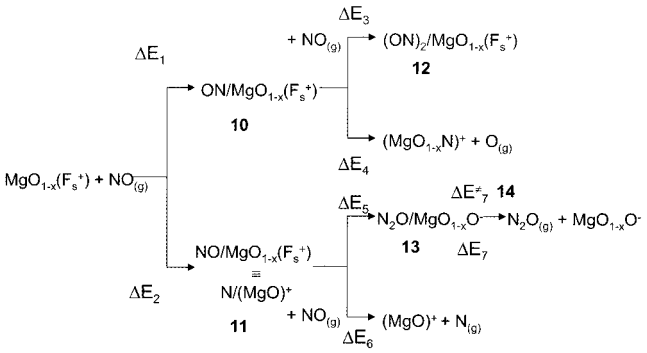

obtained for TS **5**, with a breaking NO_{ads} bond of 1.854 Å and a slightly higher NNO angle, 145° vs 134°.

We now discuss the energetics of the reaction steps, Scheme 2 and Table 1. The singlet states for the monomeric species **10a** and **11a** are both higher in energy than the triplet states, by 1.21 eV for N-down and 0.88 eV for O-down. The stabilization of the monomeric NO species on the F_s^+ center of the terrace (ΔE_1 and ΔE_2) is comparable to that of the edge F_s center but is ∼1 eV smaller than that for the terrace F_s center. Therefore, the F_s^+ centers are definitely less preferred for adsorption with respect to the neutral ones. Moreover, the addition of a second NO molecule (ΔE_3 and ΔE_5) on both N-down- and O-down-oriented species is exothermic but by only −0.49 eV for **12** and −1.28 eV for **13**. The activation barrier for the production of N_2O is higher than that calculated for the corresponding terrace F_s center by ∼0.3 eV, while the reaction energies to the products are similar: −0.18 eV vs −0.14 eV. Dissociation of the adsorbed NO by elimination of O in **10** or of N in **11** is endothermic by 5.81 and 3.57 eV, respectively.

We can conclude that the reactivity toward NO dimerization and N_2O production is partially reduced on going from the F_s center to the F_s^+ center. A clear distinction between the two sites is however not possible on the basis of the energetics of N_2O formation since the energy differences are relatively small.

3.2.5. Shallow Electron Traps. Are oxygen vacancies necessary to activate the N_2O formation? On the MgO surface one can assume the presence of other electron-trapping sites such as, for example, morphological sites or a three-coordinated Mg^{2+} cation.[21] However, these centers can probably be created only by a chemical treatment of the surface, such as doping with alkali-metal atoms or H_2 dissociation followed by UV irradiation. These methods are currently used to create paramagnetic centers on the surface of polycrystalline MgO.[52,53] These conditions do not apply to the MgO thin films considered in this study. Still, we have considered a reverse corner with a trapped electron as a representative example of a shallow electron trap.

We first analyzed the ability of the reverse corner, without any trapped electron, to bind an oxygen atom, **15**, and a NO molecule, **16** (the structural parameters in Figure 4 refer to the corresponding structures with one trapped electron).[54] An oxygen atom (in its triplet state) is bound by 1.81 eV. The NO molecule is bound by only 0.18 eV. NO dissociation is largely unfavored, $\Delta E = 4.91$ eV. The addition of a second NO molecule is not followed by dimerization, since the second NO molecule prefers to chemisorb ($D_e \approx 0.5$ eV) on a low-coordinated anion[13] rather than to form a weak bond to the first NO molecule. This was proven by geometry relaxation, with more then one set of starting positions. Therefore, we can conclude that in the absence of excess electrons dimerization is not promoted.

We looked at the EA of the reverse corner under study, to evaluate its ability to act as an electron trap.[21] In our model, the electron is bound by ∼0.5 eV. More refined calculations including the long-range polarization of the surroundings through a shell model approach give a higher value of ∼1 eV.[21] In the presence of a trapped electron the NO molecule is more tightly bound to the site, **16**, by 1.53 eV (0.18 eV in the absence of the trapped electron). In line with the results obtained for the F_s centers, direct NO dissociation starting from **16** is an endothermic process by 2.75 eV. In the presence of a trapped electron the addition of the second NO molecule leads to dimerization, **17**, with a quite strong stabilization energy, −2.66 eV. Such a value is between those calculated for the dimerization on the F_s^+ center and the neutral F_s center. Therefore, the F_s center is the preferred site for dimerization, among the electron-trapping sites considered. Moreover, on the reverse corner the NO bonds are activated to 1.263 and 1.294 Å only. Such stretching is probably not sufficient to reduce the activation barrier for the production of N_2O, whose reaction energy is calculated to be 0.38 eV.

We can conclude that shallow electron-trapping sites, such as the reverse corner, are less reactive toward NO reduction than terrace F_s centers, while they may be competitive with the low-coordinated F_s centers and the positively charged F_s^+ centers. In general, also for this type of site direct NO dissociation is definitely unfavored with respect to the process through molecular adsorption and dimerization.

3.2.6. Low-Coordinated Anionic Sites. As we mentioned in the Introduction, Zecchina and co-workers proposed the anionic site on MgO as responsible for NO dimer formation and for the consequent N_2O production.[6] NO chemisorbs on the low-coordinated oxygen anions (**18**), Figure 5, such as the oxygen anion at an edge site, with a binding energy of ∼0.5 eV.[13] A second NO molecule reacts with the chemisorbed NO molecule to form a $N_2O_3^{2-}$ surface species. This second NO is bound to the surface species by 0.95 eV; see Figure 5. One of the two N atoms is more or less at the same distance from the oxygen of the N_2O_2 molecule and that of the surface. To produce N_2O, these two bonds have to be broken and a peroxo species O_2^{2-} (**20**) should form on the surface.[54,55] The NO bonds in **19**, 1.305 and 1.388 Å, respectively, are shorter than for the dimers on the terrace F_s centers but similar to those for the dimers on the edge F_s and F_s^+ centers. To analyze the thermodynamics of the process, we take into account the energy cost of breaking the two NO bonds and the energy gain to form the peroxo bond: the final result is an endothermic process by 0.47 eV. Such energy variation is the highest observed in this work on going from an adsorbed dimer to free N_2O. This can be explained by considering that in the present case two NO bonds have to be broken instead of one as in the previous systems; moreover, these bonds are not activated as for the other cases. Thus, we conclude that low-coordinated O^{2-} sites can act as centers where N_2O formation occurs only at higher temperatures and once all the F centers have been involved in the reaction. This result is supported by isotope exchange experiments performed on polycrystalline MgO which show the formation of N_2O at the expense of lattice oxygens for temperatures in the range of 350−1000 K.[56,57]

4. Conclusions

To summarize, the following conclusions can be drawn from the analysis of the various experimental and theoretical data on the conversion reaction of NO to N_2O on MgO thin films.

(1) For all sites considered dimerization, $NO + NO \rightarrow N_2O_2$, is preferred over direct NO dissociation, $NO \rightarrow N_{ads} + O_{ads}$.

(2) On the terrace F_s centers N_2O_2 spontaneously dissociates into $O_{ads} + N_2O$ with virtually no energy barrier, 0.1 eV. This result is fully consistent with the experimental observation of N_2O formation at low temperature (120 K). Furthermore, the progressive quenching of the active F_s centers explains the reduced activity of the film, observed after subsequent exposure of the surface to NO.

(3) On edge F_s centers or charged F_s^+ centers, irrespective of the location of the site, the $N_2O_2 \rightarrow O_{ads} + N_2O$ reaction is thermoneutral or moderately exothermic, but the energy barrier, 0.4−0.7 eV, is higher than for the terrace F centers.

(4) Low-coordinated O anions favor the formation of N_2O_2 (exothermic reaction) but are not involved in the N_2O_2 to $N_2O + O_{ads}$ disproportionation at low temperature because the reaction is endothermic and the barrier is >0.5 eV. This consideration is fully supported by the ^{18}O isotope exchange experiment, according to which no ^{18}O-containing species have been detected by thermal desorption spectroscopy, at variance with high-temperature reactions on powder MgO samples where the occurrence of isotope exchange has been observed.[56,57]

(5) Shallow electron traps (morphological sites which can trap one electron) may be active in the production of N_2O but with a minor efficiency compared to oxygen vacancies. We can exclude the possibility that these morphological sites on the MgO thin film are populated by trapped electrons at the conditions at which the experiment was performed, since they should not resist annealing at elevated temperatures.

Acknowledgment. This work has been supported by the Italian INFM through the PRA ISADORA project and the University of Ulm by an HBFG grant (182-349). S.A. is supported by a postdoctoral fellowship of the Swiss National Science Foundation.

References and Notes

(1) Brown, W. A.; Gardner, P.; Perez-Jigato, M.; King, D. A. *J. Chem. Phys.* **1995**, *102*, 7277.
(2) Brown, W. A.; Gardner, P.; King, D. A. *J. Phys. Chem.* **1995**, *99*, 7065
(3) Dumas, P.; Suhren, M.; Chabal, Y. J.; Hirschmugl, J. C.; Williams, G. P. *Surf. Sci.* **1979**, *145*, 26.
(4) Masel., R. I.; Umbach, E.; Fuggle, J. C.; Menzel, D. *Surf. Sci.* **1979**, *145*, 26.
(5) Wee, A. T. S.; Lin, J.; Huan, A. C. H.; Loh, F. C.; Tan, K. L. *Surf. Sci.* **1994**, *304*, 145.
(6) Platero, E. E.; Spoto, G.; Zecchina, A. *J. Chem. Soc., Faraday Trans. 1* **1995**, *81*, 1283.
(7) Yanagisawa, Y. *Appl. Surf. Sci.* **1995**, *89*, 251.
(8) Acke, F.; Panas, I.; Strömberg, D. *J. Phys. Chem. B* **1997**, *101*, 6484.
(9) Acke, F.; Panas, I. *J. Phys. Chem. B* **1998**, *102*, 5127.
(10) Acke, F.; Panas, I. *J. Phys. Chem. B* **1999**, *103*, 2195.
(11) Snis, A.; Miettinen, H. *J. Phys. Chem. B* **1998**, *102*, 2555.
(12) Kantorovich, L. N.; Gillan, M. J. *Surf. Sci.* **1997**, *376*, 169.
(13) Di Valentin, C.; Pacchioni, G.; Chiesa, M.; Giamello, E.; Abbet, S.; Heiz, U. *J. Phys. Chem. B* **2001**, *106*, 1637.
(14) Kolmakov, A.; Stultz, J.; Goodman, D. W. *J. Chem. Phys.* **2000**, *113*, 7564.
(15) Snis, A.; Panas, I. *Surf. Sci.* **1998**, *412/413*, 477.
(16) Lu, X.; Xu, X.; Wang, N.; Zhang Q. *J. Phys. Chem. B* **1999**, *103*, 5657.
(17) McKellar, A. R. W.; Watson, J. K. G.; Howard, B. J. *Mol. Phys.* **1995**, *86*, 273. Watson, J. K. G.; McKellar, A. R. W. *Can. J. Phys.* **1997**, *75*, 181.
(18) Huber, K. P.; Herzberg, G. *Molecular Spectra and Molecular Structure, IV Constants of diatomic molecules*; Van Nostrand Reinhold: New York, 1979.
(19) Duarte, H. A.; Proynov, E.; Salahub, D. R. *J. Chem. Phys.* **1998**, *109*, 26.
(20) Snis, A.; Panas, I. *Chem. Phys.* **1997**, *221*, 1.
(21) Ricci, D.; Pacchioni, G.; Shusko, P.; Shluger, A. To be published.
(22) Heiz, U.; Vanolli, F.; Trento, L.; Schneider, W.-D. *Rev. Sci. Instrum.* **1997**, *68*, 1986.
(23) Schaffner, M.-H.; Patthey, F.; Schneider, W.-D. *Surf. Sci.* **1998**, *417*, 159.
(24) Wu, M.-C.; Corneille, J. S.; He, J.-W.; Estrada, C. A.; Goodman, D. W. *J. Vac. Sci. Technol., A* **1992**, *10*, 1467.
(25) Wu, M.-C.; Corneille, J. S.; Estrada, C. A.; He, J.-W.; Goodman, D. W. *Chem. Phys. Lett.* **1991**, *182*, 472.
(26) Liehr, M.; Thiry, P. A.; Pireaux, J. J.; Caudano, R. *Phys. Rev. B* **1986**, *33*, 5682.
(27) Tjeng, L. H.; Vos, A. R.; Sawatzky, G. A. *Surf. Sci.* **1990**, *235*, 269.
(28) He, J.-W.; Møller, P. L. *Chem. Phys. Lett.* **1986**, *129*, 13.
(29) Nygren, M. A.; Petterson, L. G. M. *J. Chem. Phys.* **1996**, *105*, 9339.
(30) He, J.-W.; Cesar, A. E.; Corneille, J. S.; Wu, M.-C.; Goodman, D. W. *Surf. Sci.* **1992**, *261*, 167.
(31) Wichtendahl, R.; Rodriguez-Rodrigo, R.; Härtel, U.; Kuhlenbeck, H.; Freund, H.-J. *Surf. Sci.* **1999**, *423*, 90.
(32) Wichtendahl, R.; Rodriguez-Rodrigo, R.; Härtel, U.; Kuhlenbeck, H.; Freund, H.-J. *Phys. Status Solidi A* **1999**, *173*, 93.
(33) Abbet, S.; Riedo, E.; Brune, H.; Heiz, U.; Ferrari, A. M.; Giordano, L.; Pacchioni, G. *J. Am. Chem. Soc.* **2001**, *123*, 6172−6178.
(34) Heiz, U.; Schneider, W.-D. *J. Phys. D: Appl. Phys.* **2000**, *33*, R85.
(35) *Cluster Models for Surface and Bulk Phenomena*; Pacchioni, G., Bagus, P. S., Parmigiani, F., Eds.; NATO ASI Series B, Vol. 283; Plenum: NewYork, 1992.
(36) Sauer, J.; Ugliengo, P.; Garrone, E.; Saunders: V. R. *Chem. Rev.* **1994**, *94*, 2095.
(37) Colbourn, E. A. *Surf. Sci. Rep.* **1992**, *15*, 281.
(38) Pacchioni, G.; Ferrari, A. M.; Marquez, A. M.; Illas, F. *J. Comput. Chem.* **1997**, *18*, 617.
(39) Ferrari, A. M.; Pacchioni, G. *Int. J. Quantum Chem.* **1996**, *58*, 241.
(40) Cundari, T. R.; Stevens, W. J. *J. Chem. Phys.* **1993**, *98*, 5555.
(41) Stevens, W. J.; Basch, H.; Krauss, M. *J. Chem. Phys.* **1984**, *81*, 6026.
(42) Winter, N. W.; Pitzer, R. M. *J. Chem. Phys.* **1988**, *89*, 446.
(43) Nygren, M. A.; Petterson, L. G. M.; Barandiaran, Z.; Seijo, L. *J. Chem. Phys.* **1994**, *100*, 2010.
(44) Mejias, J. A.; Marquez, A. M.; Fernandez Sanz, J.; Fernandez-Garcia, M.; Ricart, J. M.; Sousa, C.; Illas, F. *Surf. Sci.* **1995**, *327*, 59.
(45) Pacchioni, G. *Heterog. Chem. Rev.* **1995**, *2*, 213.
(46) Becke A. D. J. *J. Chem. Phys.* **1993**, *98*, 5648.
(47) Lee, C.; Yang, W.; Parr, R. G. *Phys. Rev. B* **1988**, *37*, 785.
(48) Ferrari, A. M.; Soave, R.; D'Ercole, A.; Pisani, C.; Giamello, E.; Pacchioni, G. *Surf. Sci.* **2001**, *479*, 83.
(49) Frisch, M. J.; et al. *Gaussian 98*; Gaussian Inc.: Pittsburgh, PA, 1997.
(50) Sanchez, A.; Abbet, S.; Heiz, U.; Schneider, W.-D.; Häkkinen, H.; Barnett, R. N.; Landman, U. *J. Phys. Chem. A* **1999**, *103*, 9573.
(51) Ferrari, A. M.; Giordano, L.; Pacchioni, G.; Abbet, S.; Heiz, U. *J. Phys. Chem. B*, in press.
(52) Giamello, E.; Ferrero, A.; Coluccia, S.; Zecchina, A. *J. Phys. Chem.* **1991**, *95*, 9385.
(53) Tench, A. J. *Surf. Sci.* **1971**, *25*, 625.
(54) Kantorovich, L. N.; Gillan, M. J. *Surf. Sci.* **1997**, *374*, 373.
(55) Snis, A.; Panas, I. *J. Chem. Phys.* **1995**, *103*, 7626.
(56) Yanagisawa, Y. *Appl. Surf. Sci.* **1995**, *89*, 251.
(57) Yanagisawa, Y.; Yamabe, S.; Matsumura, K.; Huzimura, R. *Phys. Rev. B* **1993**, *48*, 4925.